Analyst

An Electro-Mechano-Optical NMR probe for ^{1}H-^{13}C double resonance in a superconducting magnet

Journal:	*Analyst*
Manuscript ID	AN-ART-02-2022-000220.R1
Article Type:	Paper
Date Submitted by the Author:	09-Mar-2022
Complete List of Authors:	Tominaga, Yusuke; Kyoto University, Division of Chemistry, Graduate School of Science Takeda, Kazuyuki; Kyoto University, Division of Chemistry, Graduate School of Science

Journal Name

ARTICLE TYPE

Cite this: DOI: 00.0000/xxxxxxxxxx

An Electro-Mechano-Optical NMR probe for ^{1}H-^{13}C double resonance in a superconducting magnet

Yusuke Tominaga[a] and Kazuyuki Takeda*[a]

Received Date
Accepted Date

DOI: 00.0000/xxxxxxxxxx

Electro-Mechano-Optical (EMO) NMR, an emerging NMR detection technique with signal upconversion from radiofrequency to optical regimes via Si_3N_4 nanomembrane, has become compatible with NMR analysis in chemistry using a highly homogeneous but space-limited magnetic field provided by a superconducting magnet (SCM) by development of a compact EMO NMR probe operational inside the SCM bore. Optical ^{13}C NMR signal detection following ^{1}H-^{13}C magnetization transfer in liquid benzene is demonstrated.

1 Introduction

Nuclear Magnetic Resonance (NMR) is an indispensable analytical tool in chemistry and biochemistry, providing a probe for the structure and dynamics in materials of interest. The major challenge in NMR has been the low sensitivity. One direction toward improving the signal-to-noise ratio (SNR) is nuclear hyperpolarization, in which highly biased, non-equilibrium population distribution over the Zeeman energy levels is created by dynamic nuclear polarization[1–5], optical pumping[6–16], para-hydrogen[17–20], methyl-group quantum rotors[21–27], and so on. Another direction is to improve the detection sensitivity, one straightforward way of which is to cool the circuit down to cryogenic temperatures to reduce Johnson noise[28–31].

In the context of the latter, we recently reported what we call Electro-Mechano-Optical (EMO) NMR[32,33], by applying the idea of signal transduction from radiofrequency (rf) to optical regimes using a metal-coated, nanomembrane oscillator[34,35]. In EMO NMR, the metal layer on the membrane plays two roles, namely, an optical mirror and an electrode of a capacitor forming a resonant circuit with an inductor[32,33,36,37]. In the presence of the electro-mechanical coupling, the electromotive force that develops in the circuit due to nuclear induction causes amplitude modulation of membrane's oscillation. In turn, the membrane's displacement is read out by an optical means. This strategy potentially leads to better detection sensitivity compared to that of the conventional, electrical detection of NMR, provided that the efficiency of signal transduction from the electric circuit to the mechanical oscillator is optimized[32]. That is, noise added through the process of signal transduction can be made smaller. Ultimately, the performance of the EMO signal transduction can correspond to that of the conventional scheme with a noiseless, but unrealistic, preamplifier. Even though EMO NMR involves mechanics, it differs from magnetic-resonance force microscopy (MRFM)[38–40] in that the former is potentially applicable to various types of samples, as long as they fit in the detection coil.

Even though proof-of-principle demonstrations of EMO NMR were successful[32,33], these early works used a desktop permanent magnet and optical components aligned on a massive optical bed, and were incompatible with NMR studies dedicated for chemical analysis, where a high and very homogeneous magnetic field provided by a superconducting magnet (SCM) is usually used. Indeed, modern high-resolution NMR systems use magnetic fields of as high as several Tesla or even higher. In addition, the requirement for the magnetic-field inhomogeneity, lower than 10^{-7}, is remarkable. State-of-art SCMs produce such high and homogeneous magnetic fields inside a narrow (several centimeters in diameter) cylindrical region. To access the sweet spot, one needs to put the sample and the detection circuit deep (several tens of centimeters) into the bore of the SCM. That is why thin and long NMR *probes* are mandatory. Here, we report design and fabrication of an EMO NMR probe dedicated for ^{1}H-^{13}C double resonance experiments with a SCM, and demonstrate ^{1}H-^{13}C magnetization transfer by INEPT (insensitive nuclei enhanced by polarization transfer)[41–44] followed by EMO detection of ^{13}C NMR signals.

2 EMO NMR Probe

A commercially available Si_3N_4 membrane with a lateral size of 1 mm $\times$ 1 mm and thickness of 200 nm, supported by a 5 mm $\times$ 5 mm Si-frame, was used to make the rf-to-light transducer. An aluminum layer was vacuum deposited on the membrane (Fig. 1(a)). A 5 mm $\times$ 5 mm, double-sided printed circuit board (PCB) was employed for the counter electrode of the capacitor. By aluminum vacuum deposition, 500 nm high, four pillars were

[a] *Division of Chemistry, Graduate School of Science, Kyoto University, 606-8502 Kyoto, Japan.*
* E-mail: takezo@kuchem.kyoto-u.ac.jp

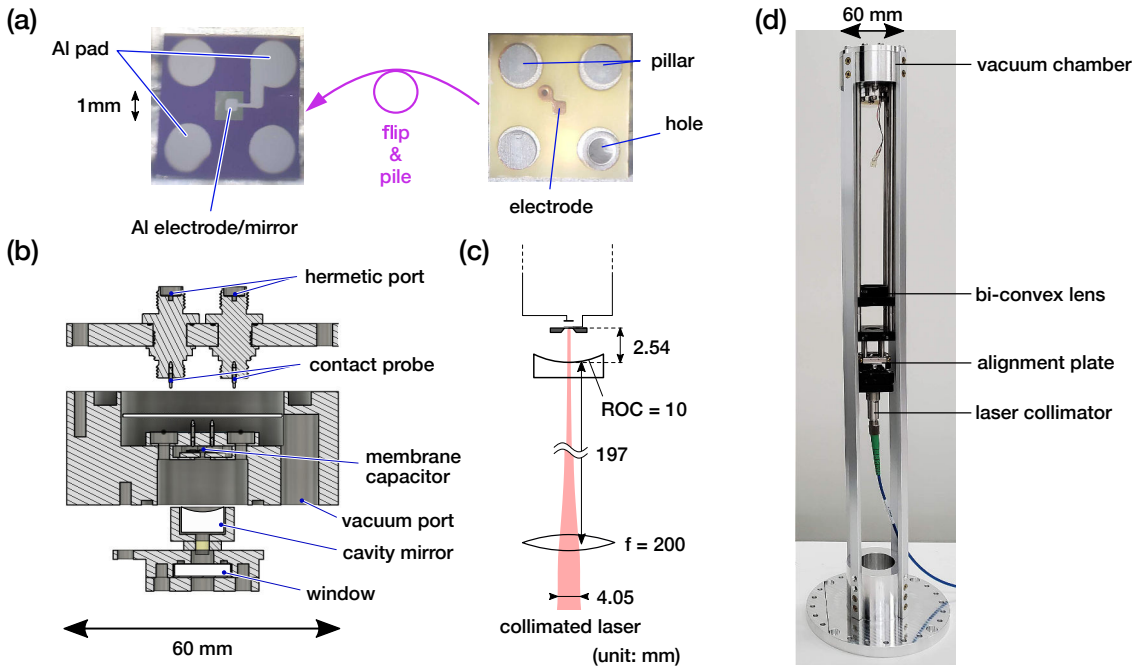

Fig. 1 (a) (top) A 5 mm × 5 mm Si frame supporting a 1 mm × 1 mm Si_3N_4 membrane at its center, on which an aluminum layer for the capacitor electrode and the optical mirror was made by vacuum deposition. Four pads were also made on the frame with the same thickness as that on the membrane. (bottom) A printed circuit board serving for the counter electrode of the membrane capacitor, which was piled on the Si frame. The gap of the capcitor was adjusted to ca. 500 nm by making pillars by vacuum deposition. (b) Cross sectional view of a cylindrical vacuum chamber containing the membrane capacitor. (c) Design of the optical cavity for a collimated laser beam with an incident beam diameter of 4.05 mm. A concave mirror with a radius of curvature (ROC) of 10 mm and a lens with a focal length (f) of 200 mm were combined to form the cavity with a length of 2.54 mm. (d) A snapshot of the assembled probe for EMO NMR compatible with the SCM, where the optical components are vertically aligned.

build on the PCB, which was then piled on the Si membrane frame. To avoid air damping, the membrane was put in a home-made, palmtop-sized vacuum chamber. Typically, the room inside the chamber is evacuated down to ca. 1 Pa using a turbo molecular pump.

Figure 1(b) shows a schematic cross sectional view of the chamber with a diameter of 60 mm, which can be inserted into standard widebore SCMs. To minimize the wiring length inside the chamber, a pair of hermetically sealed ports employed on the lid were arranged such that contact probes gently push the pads connected electrically to the electrodes of the membrane capacitor.

To let the aluminum layer on the membrane work in the optical part as well, a concave cavity mirror with radius of curvature (ROC) of 10 mm was employed inside the vacuum chamber. A laser beam with a wavelength of 1064 nm, guided through and out of an optical fiber, was collimated, focused, and then led through the chamber window into the optical cavity. The profile of the laser beam was designed as shown in Fig. 1(c) based on paraxial wave optics. Here, the cavity length of 2.54 mm was intended to be as short as possible to make the system robust against optical misalignment. The laser beam was mode-matched in such a manner that its waist with a diameter of 76.8 μm is located on the mirror on the membrane, and the curvature of the wavefront matches that of the cavity mirror at its concave surface. In addition, we did our best to optimize optical alignment, by gently tightening/loosening the screws used to fix the window-holding plate to the body of the vacuum chamber. We found that the O-ring between the plate and the chamber body, originally employed for the sealing purpose, also served effectively for non-magnetic springs without vacuum being broken.

As shown in Fig. 1(d), the collimator, the convex lens, and the optical cavity were aligned vertically, so that they could be inserted into the SCM bore. The collimator was supported by a tilt/positioning plate used to adjust alignment of the incident laser beam.

3 Experimental

Figure 2(a) describes a diagram of the experimental setup for ^{1}H-^{13}C double resonance NMR with ^{13}C EMO detection functionality. In addition to excitation rf pulses at the ^{1}H and ^{13}C resonance frequencies with arbitrary amplitude and phase modulations, the drive signal needs to be applied with its frequency being either the sum or the difference in the frequency of ^{13}C resonance (50.344566 MHz) and that of characteristic oscillation of the membrane (387.835 kHz). To apply both rf pulses and the drive signal, we used an open-source, home-built NMR spectrometer[45–47], which was modified to enable implementation of EMO NMR as well as the conventional pulse sequences. In the ^{13}C transmitter, the carrier signal is fanned out into two, and one is dedicated for the conventional NMR excitation, while the other is used to generate tone signals for testing purposes.

A saddle coil was used for exciting the ^{1}H and ^{13}C spins in the sample in a magnetic field of 4.7 T, while a solenoid coil was employed for EMO ^{13}C NMR detection. The saddle coil was doubly-

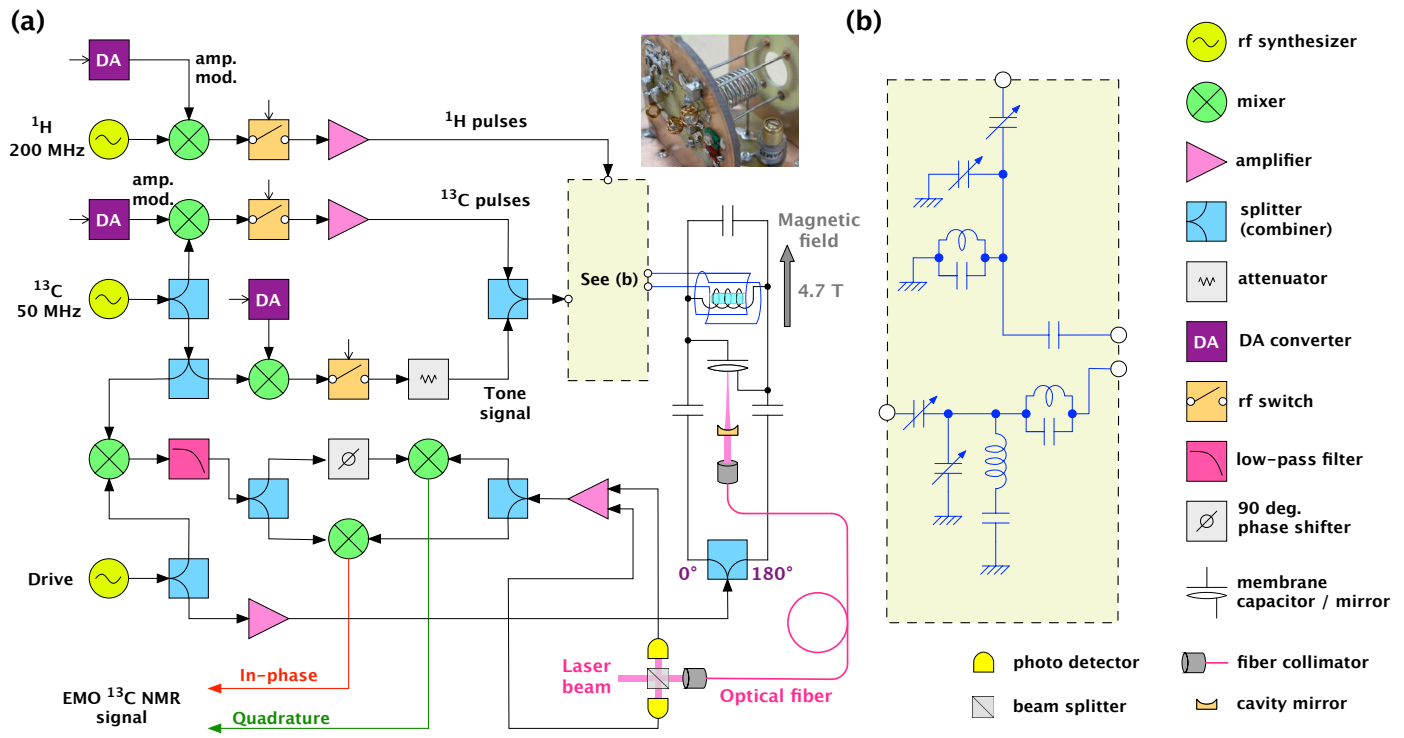

Fig. 2 (a)A diagram describing the experimental setup. (b)A circuit diagram for ^{1}H-^{13}C double-resonance NMR.

tuned at ca. 200 MHz and ca. 50 MHz, which correspond to the ^{1}H and ^{13}C resonances. The circuit diagram for the single-coil double resonance circuit is depicted in Fig. 2(b).

The solenoid coil for EMO ^{13}C NMR detection formed a tank circuit with the membrane capacitor connected in parallel. With the help of another shunt capacitor, the resonance frequency was adjusted to that of ^{13}C NMR. The drive signal, passing through a 180° splitter, comes into the resonant circuit in the differential mode through a pair of impedance-matching capacitors.

The electromotive force developing across the terminals of the solenoid coil due to ^{13}C nuclear induction causes the Coulomb force between the electrodes of the membrane capacitor, changing the amplitude of characteristic oscillation of the membrane in the presence of the drive signal at 50.732401 MHz. In turn, the amplitude of the laser beam reflecting back from the optical cavity is also modulated. In this way, the NMR signal can surf on the optical carrier. The reflected laser beam is sent to a photo-detector. Another photo-detector is employed to monitor the incident laser beam. Differential amplification of these optical signals leads to shot-noise limited photo-detection. In the system, the ^{13}C carrier signal and the drive signal is mixed to generate the coherent reference signal at the mechanical frequency, which is used for quadrature demodulation of the optical signal that carries the light-converted NMR signal at the membrane's mechanical frequency at 387.835 kHz.

We implemented ^{1}H-^{13}C double resonance, refocused INEPT[41–44] experiments with ^{13}C observation under ^{1}H decoupling in ^{13}C-labeled benzene in the liquid state. In this pulse sequence, described in Fig. 3(a), polarization is transferred from the ^{1}H spins to the J-coupled ^{13}C spins, and the ^{13}C spin echo following an inversion pulse is detected under ^{1}H decoupling. The pulse sequence used here is popular and standard in modern liquid-state NMR, except for the application of the drive signal that is required for rf-to-light signal conversion. To prevent strong rf pulses from being transduced, the frequency of the drive signal was temporary switched by 400 kHz during pulse excitation.

4 Results

Figure. 3(b)(c) shows an optically detected, refocused-INEPT-enhanced ^{13}C FID acquired in ^{13}C labeled benzene and its Fourier-transformed spectrum. Here, the drive signal at 50.732401 MHz, which was the sum of the ^{13}C resonance frequency and the membrane's characteristic oscillation frequency, was applied with power of 26.3 dBm. The power of the incident laser beam into the optical cavity was set to 1.1 mW. In the sense that the up-converted optical signal has successfully been acquired using the SCM in combination with the widely-used, ^{1}H-^{13}C double-resonance pulse sequence, this result has opened the way toward the applications of EMO detection to NMR for chemical/biochemical analyses.

For comparison, the ^{13}C signal and the spectrum acquired by the conventional, electrical method under application of the identical pulse sequence is shown in Fig. 3(d)(e). The profiles of the time domain signals and the spectra are virtually identical for EMO NMR and the conventional NMR. The somewhat different appearances of noise are ascribed to the difference in the bandwidth of the detectors. In EMO NMR, the detection bandwidth is limited by that of the membrane oscillator, whereas in the conventional NMR with electrical detection, the bandwidth is given by that of the resonant circuit. In our case, the former

was ca. 100 Hz, which is rather narrow compared to the typical ^{13}C chemical shifts ranging by ca. 200 ppm, which, in the present magnetic field of 4.7 T, correspond to ca. 10 kHz. The detection bandwidth may be made wider in several ways. One straightforward approach would be to decrease the degree of vacuum in the chamber where the membrane oscillator sits, so as to increase the effect of air damping. However, gaining the bandwidth by introducing loss would sacrifice the sensitivity. Accordingly, our future direction toward wideband EMO NMR would be to increase the coupling strengths between the membrane oscillator and both the electrical and the optical systems. In particular, the gain in the bandwidth with the enhanced electro-mechanical coupling is favorable, as it would also lead to the enhanced efficiency in the signal transduction from the electrical to the mechanical systems. Reducing the gap between the electrodes of the membrane capacitor would effectively improve the electro-mechanical coupling strength[32].

By increasing the electro-mechanical coupling strength, the signal and Johnson noise transduced to the membrane oscillator increase by the same amount. As the coupling strength is further increased, the Johnson noise transduced to the mechanical system eventually exceeds the noise due to the Brownian motion of the membrane oscillator. Since the noise associated with the optical part of the system is much lower, the overall signal-to-noise ratio is ultimately limited by the Johnson noise alone for a given temperature of the experimental system, when the electro-mechanical coupling strength can be made sufficiently larger. The Johnson noise that develops in the resonant circuit is unavoidable and contribute to both EMO NMR and the conventional NMR at a given temperature. In the latter, conversely, additional noise is inevitably caused by the preamplifier.

To compare the sensitivity of the EMO detection using the current experimental setup with that of the conventional electrical detection, we applied a synthesized, continuous-wave tone signal at 50.34455 MHz to the solenoid coil through the saddle coil, which coupled to the former through weak but finite mutual inductance. Fig. 4(a) shows a power spectrum of the optically detected tone signal with power of −121.6 dBm under application of the drive signal at 50.73273 MHz with power of 26.3 dBm, where the light-converted tone signal appear as a sharp peak on the relatively broad, Lorentzian profile which reflects the Brownian motion of the membrane at its characteristic frequency of the fundamental mode at 388.18 kHz. Conversely, the power spectrum shown in Fig. 4(b) was obtained by switching off the drive signal, and then by electrically amplifying the tone signal coming out of the drive circuit using a low-noise amplifier with noise figure of 1.1 dB. Here, the data in Fig. 4 were normalized to the height of the tone signal.

In the case of optical detection, the floor of noise at the frequency of the tone signal is given by the height of the Lorentzian component associated with the Brownian motion of the membrane oscillator. Thus, the noise floor at this specific frequency was higher than that of the electrically detected signal. Nevertheless, at frequencies outside the bandwidth of the membrane's characteristic oscillation, the noise floor in the power spectrum of the optically detected signal was lower compared to that of the

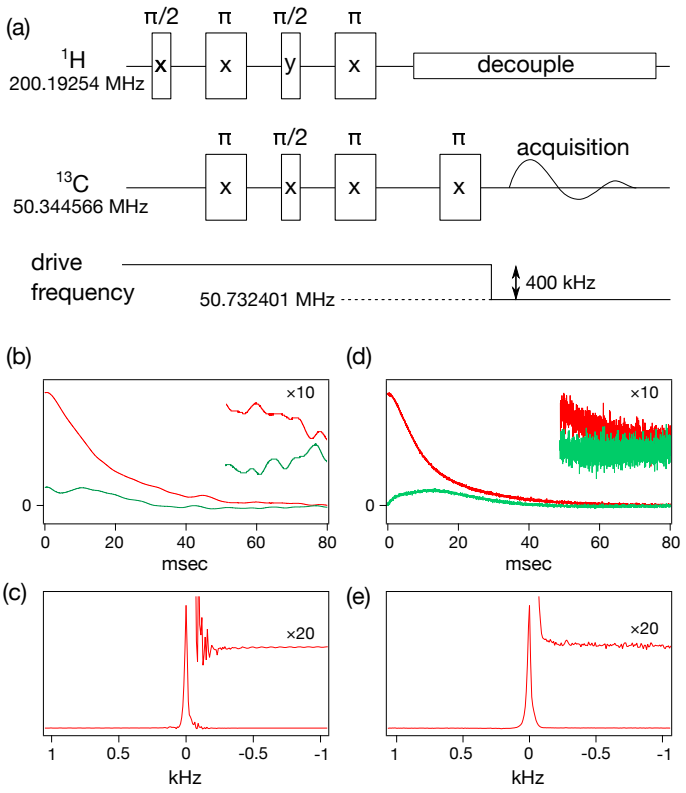

Fig. 3 (a) A pulse sequence for refocused INEPT with ^{1}H decoupling. The timing of switching the frequency of the drive signal, employed to prevent the excitation pulse from being transduced, is also described in the diagram. (b)(c) A refocused INEPT enhanced ^{13}C NMR signal and Fourier-transformed spectrum of ^{13}C-labeled benzene obtained by the EMO NMR scheme with the power of the drive signal of 26.3 dBm. The power of the laser beam for optical readout was 1.1 mW. The in-phase and the quadrature components of the demodulated signal are shown in red and green lines, respectively. (d)(e) The ^{13}C signal and spectrum of the same sample obtained by the conventional electrical detection using the same pulse sequence. In both (b) and (d), the signals were accumulated over 40 times at room temperature in a nominally 4.7 T SCM. The ^{1}H and ^{13}C resonance frequencies were 200.19254 MHz and 50.344566 MHz.

electrically detected one, as seen in Fig. 4. This indicates that the signal-to-noise ratio of the EMO scheme potentially exceeds that of the electrical detection, by reducing the relative contribution of the Brownian noise. As mentioned above, increasing the electro-mechanical coupling is effective. In addition, the Brownian noise would be reduced by lowering the temperature of the membrane oscillator. Another option in favor of ambient temperature operation would be to implement radiation-pressure induced laser cooling of the membrane oscillator[48–52]. Toward this end, the intensity of the laser beam needs to be much larger than that used in this work. Then, however, with the current aluminum mirror on the membrane, light absorption of even a few percent by the aluminum cause serious heating, even though we intend to implement laser cooling. In this context, metasurface mirrors built in the membrane is promising[53–55]. Indeed, we have recently developed an rf-to-light transducer using the optically loss-less, heating-free metasurface mirror[56], which can be applied to EMO NMR detection under laser cooling of the membrane oscillator in

the future.

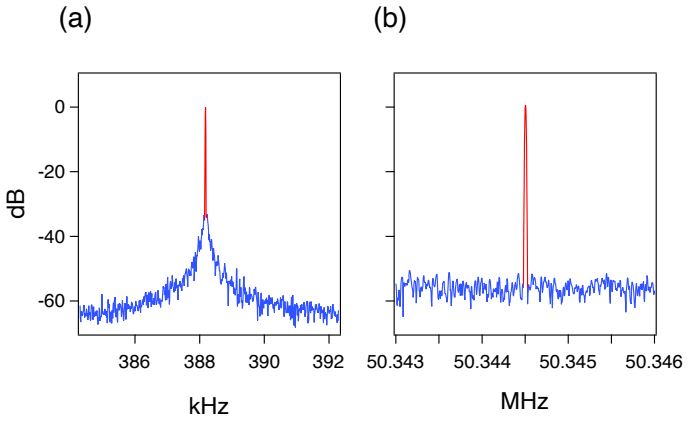

Fig. 4 (a) A power spectrum of an optical signal around the frequency 388.18 kHz of membrane's characteristic oscillation. The signal was acquired under application of a tone signal at 50.3445 MHz with power of -121.6 dBm and a drive signal at 50.7339 MHz with power of 18 dBm. The component that corresponds to the tone signal is drawn with the red line. (b) A power spectrum of an electrical signal obtained by amplifying the same tone signal that comes out of the resonant circuit through the sum port of the 180° splitter with a low-noise amplifier with noise figure of 1.1.

5 Conclusions

EMO NMR, which has so far been the subject in physics, has now come into the realm of NMR in chemistry with the SCM-compatible probe presented in this work. Future direction is real application to chemical analyses, and development of EMO probes for various purposes, including ^{2}H-lock integration, triple-resonance NMR solid-state magic angle spinning NMR, nuclear hyperpolarization, and magnetic resonance imaging (MRI).

Conflicts of interest

There are no conflicts to declare.

Acknowledgements

We are grateful to Koji Usami for fruitful discussions. This work has been supported by JST CREST (Grant Number JPMJCR1873), MEXT Quantum Leap Flagship Program (MEXT Q-LEAP) (Grant Number JPMXS0120330644), JSPS KAKENHI (Grant Number 18H04165), and Grants-in-Aid for JSPS Fellows (Grant Number 20J14033).

Notes and references

1 A. Overhauser, *Physical Review*, 1953, **92**, 411–415.
2 T. Carver and C. Slichter, *Physical Review*, 1953, **92**, 212–213.
3 A. Abragam, *Principle of Nuclear Magnetism*, Oxford University Press, 1961.
4 A. Abragam and M. Goldman, *Reports on Progress in Physics*, 1978, **41**, 395–467.
5 C. P. Slichter, *Reports on Progress in Physics*, 2014, **77**, 072501.
6 S. Barrett, R. Tycko, L. Pfeiffer and K. West, *Physical Review Letters*, 1994, **72**, 1368–1371.
7 S. E. Barrett, G. Dabbagh, L. N. Pfeiffer, K. W. West and R. Tycko, *Physical Review Letters*, 1995, **74**, 5112–5115.
8 R. Tycko, S. Barrett, G. Dabbagh, L. Pfeiffer and K. West, *Science*, 1995, **268**, 1460–1463.
9 R. Tycko, *Solid State Nuclear Magnetic Resonance*, 1998, **11**, 1–9.
10 C. Michal and R. Tycko, *Physical Review B*, 1999, **60**, 8672–8679.
11 K. L. Sauer, C. A. Klug, J. B. Miller and J. P. Yesinowski, *Physical Review B - Condensed Matter and Materials Physics*, 2011, **84**, 1–12.
12 G. Navon, Y.-Q. Song, T. Room, S. Appelt, R. E. Taylor and A. Pines, *Science*, 1996, **271**, 1848–1851.
13 M. S. Albert, G. D. Cates, B. Driehuys, W. Happer, B. Saam, C. S. Springer and A. Wishnia, *Nature*, 1994, **370**, 199–201.
14 H. W. Long, H. C. Gaede, J. Shore, L. Reven, C. R. Bowers, J. Kritzenberger, T. Pietrass, A. Pines, P. Tang and J. A. Reimer, *Journal of the American Chemical Society*, 1993, **115**, 8491–8492.
15 R. Tycko and J. A. Reimer, *The Journal of Physical Chemistry*, 1996, **100**, 13240–13250.
16 T. Pietraβ, A. Bifone, T. Rõõm and E. Hahn, *Physical Review B*, 1996, **53**, 4428–4433.
17 C. Russel and D. P. Weitekamp, *Journal of the American Chemical Society*, 1987, **109**, 5541–5542.
18 M. Goldman, H. Jóhannesson, O. Axelsson and M. Karlsson, *Magnetic Resonance Imaging*, 2005, **23**, 153–157.
19 T. Theis, P. Ganssle, G. Kervern, S. Knappe, J. Kitching, M. P. Ledbetter, D. Budker and A. Pines, *Nature Physics*, 2011, **7**, 571–575.
20 M. Anwar, D. Blazina, H. Carteret, S. Duckett, T. Halstead, J. Jones, C. Kozak and R. Taylor, *Physical Review Letters*, 2004, **93**, 2–5.
21 M. Tomaselli, C. Degen and B. H. Meier, *The Journal of Chemical Physics*, 2003, **118**, 8559.
22 A. J. Horsewill, *Progress in Nuclear Magnetic Resonance Spectroscopy*, 1999, **35**, 359–389.
23 M. Tomaselli, U. Meier, B. H. Meier and C. Zu, *Journal of Chemical Physics*, 2004, **120**, 4051–4054.
24 J. Haupt, *Physics Letters A*, 1972, **38**, 389–390.
25 S. Clough, *Physics Letters A*, 1973, **42**, 371–372.
26 M. Icker and S. Berger, *Journal of Magnetic Resonance*, 2012, **219**, 1–3.
27 J. Haupt, *Z. Naturforsch*, 1973, **28a**, 98–104.
28 P. Styles, N. Soffe, C. Scott, D. Crag, F. Row, D. White and P. White, *Journal of Magnetic Resonance*, 1984, **60**, 397–404.
29 P. Styles, N. F. Soffe and C. A. Scott, *Journal of Magnetic Resonance*, 1989, **84**, 376–378.
30 T. Mizuno, K. Hioka, K. Fujioka and K. Takegoshi, *Review of Scientific Instruments*, 2008, **79**, 044706.
31 K. R. Thurber and R. Tycko, *Journal of Magnetic Resonance*, 2008, **195**, 179–186.
32 K. Takeda, K. Nagasaka, A. Noguchi, R. Yamazaki, Y. Nakamura, E. Iwase, J. M. Taylor and K. Usami, *Optica*, 2018, **5**, 152.

33 Y. Tominaga, K. Nagasaka, K. Usami and K. Takeda, *Journal of Magnetic Resonance*, 2019, **298**, 6–15.

34 R. W. Andrews, R. W. Peterson, T. P. Purdy, K. Cicak, R. W. Simmonds, C. A. Regal and K. W. Lehnert, *Nature Physics*, 2014, **10**, 321–326.

35 T. Bagci, A. Simonsen, S. Schmid, L. G. Villanueva, E. Zeuthen, J. Appel, J. M. Taylor, A. Sørensen, K. Usami, A. Schliesser and E. S. Polzik, *Nature*, 2014, **507**, 81–85.

36 A. Simonsen, J. D. Sánchez-Heredia, S. A. Saarinen, J. H. Ardenkjær-Larsen, A. Schliesser and E. S. Polzik, *Scientific Reports*, 2019, **9**, 18173.

37 A. Simonsen, S. A. Saarinen, J. D. Sanchez, J. H. Ardenkjær-Larsen, A. Schliesser and E. S. Polzik, *Optics Express*, 2019, **27**, 18561.

38 J. Sidles, *Applied Physics Letters*, 1991, **58**, 2854–2856.

39 D. Rugar, O. Züger, S. Hoen, C. Yannoni, H.-M. Vieth and R. Kendrick, *Science*, 1994, **264**, 1560–1563.

40 D. Rugar, R. Budakian, H. Mamin and B. Chui, *Nature*, 2004, **430**, 329–332.

41 G. A. Morris and R. Freeman, *Journal of the American Chemical Society*, 1979, **101**, 760–762.

42 G. A. Morris, *Journal of Magnetic Resonance (1969)*, 1980, **41**, 185–188.

43 G. A. Morris, *Journal of the American Chemical Society*, 1980, **102**, 428–429.

44 D. Burum and R. Ernst, *Journal of Magnetic Resonance (1969)*, 1980, **39**, 163–168.

45 K. Takeda, *The Review of scientific instruments*, 2007, **78**, 033103.

46 K. Takeda, *Journal of Magnetic Resonance*, 2008, **192**, 218–229.

47 K. Takeda, *Annual Reports on NMR Spectroscopy*, 2011, **74**, 355–393.

48 P. Cohadon, A. Heidmann and M. Pinard, *Physical Review Letters*, 1999, **83**, 3174–3177.

49 S. Gigan, H. R. Böhm, M. Paternostro, F. Blaser, G. Langer, J. B. Hertzberg, K. C. Schwab, D. Bäuerle, M. Aspelmeyer and A. Zeilinger, *Nature*, 2006, **444**, 67–70.

50 D. Kleckner and D. Bouwmeester, *Nature*, 2006, **444**, 75–78.

51 O. Arcizet, P.-F. Cohadon, T. Briant, M. Pinard and A. Heidmann, *Nature*, 2006, **444**, 71–4.

52 A. Schliesser, P. Del'Haye, N. Nooshi, K. Vahala and T. Kippenberg, *Physical Review Letters*, 2006, **97**, 243905.

53 S. Fan and J. D. Joannopoulos, *Physical Review B - Condensed Matter and Materials Physics*, 2002, **65**, 1–8.

54 X. Chen, C. Chardin, K. Makles, C. Caër, S. Chua, R. Braive, I. Robert-Philip, T. Briant, P.-F. Cohadon, A. Heidmann, T. Jacqmin and S. Deléglise, *Light: Science & Applications*, 2017, **6**, e16190–e16190.

55 J. Hu, S. Bandyopadhyay, Y. H. Liu and L. Y. Shao, *Frontiers in Physics*, 2021, **8**, 1–20.

56 Y. Tominaga, A. Mikami, A. Iwamura, K. Usami and K. Takeda, *Applied Physics Express*, 2022, **15**, 012003.